Light-force-induced fluorescence line-center shifts in high-precision optical spectroscopy: Simple model and experiment

M. Artoni,[1] I. Carusotto,[1,2] and F. Minardi[1]
[1]*INFM–European Laboratory of Non-Linear Spectroscopy (LENS), Largo E. Fermi 2, I-50125 Firenze, Italy*
[2]*Scuola Normale Superiore and INFM, Piazza dei Cavalieri 7, I-56126 Pisa, Italy*
(Received 1 November 1999; published 17 July 2000)

We calculate the effect of light-induced forces on the fluorescence line shape of a two-level atom crossing at right angles two counterpropagating light beams of parallel linear polarizations (lin ∥ lin) in a common configuration for ultrahigh-precision optical spectroscopy. For an incident atomic beam with a narrow spread of transverse velocities the dipole force induces a redshift of the fluorescence maximum, while in the reverse case of a wide spread of transverse velocities the radiation-pressure force induces a blueshift of the saturation dip minimum. We then use our theory to explain the blueshift of the saturation line-center dip occurring for the closed transition $2\,^3S_1 \rightarrow 2\,^3P_2$ of a ^{4}He beam. The observed shift, which is in quite good agreement with the theory, can be of the order of 1/10 of the transition natural linewidth and hence quite important for ultrahigh-precision spectroscopy measurements.

PACS number(s): 42.50.Vk, 32.70.Jz

I. INTRODUCTION

The precise separation between atomic energy levels is typically measured by means of high-precision optical spectroscopy techniques in which one looks for absorption or the subsequent fluorescence from a sample of atoms illuminated by a laser beam. For sufficiently heavy atomic species the translational degrees of freedom are not affected by the interaction with the laser light during typical experimental times, and the incident position and momentum distribution of the atoms remains constant as the atoms move across the beam. Most spectroscopic measurements can be rather well described within this limit.

There are situations, however, in which even quite small modifications of the incident atomic distribution caused by light forces can give rise to sizable asymmetries and line-center shifts of the absorption or the fluorescence line-shape profiles, as long anticipated by the theoretical work of Kazantsev and co-workers [1]. Deformations are likely to occur for a configuration in which the atomic sample interacts with a traveling-wave laser beam. The absorption of a photon from a unidirectional light beam and subsequent emission in a random direction by spontaneous emission transfers to the atom a nonvanishing average momentum. This modifies the atomic distribution function $f(\mathbf{r},\mathbf{p},t)$ and leads in turn to appreciable changes in the refractive [2–4] and absorptive [5] properties.

The effect is less obvious, however, for spectroscopic configurations in which the atoms from a well-collimated beam cross at right angles two counterpropagating laser beams of equal intensities. The effects of the two beams are expected to compensate each other so that the atoms' average velocity along the laser beam axis will remain zero by symmetry: no Doppler shift (due to no net deflection) is expected to modify the atomic distribution and hence the absorption or fluorescence profiles [6]. Yet, even for this specific configuration, line-center shifts induced by light forces can take place as first observed experimentally by Prentiss and Ezekiel [7]. In this experiment, in particular, the shift was attributed to the dipole force experienced by the induced atomic dipole in the field gradient of the standing wave and a rather preliminary estimate of the shift effect was put forward.

Many of the spectroscopic measurements of transition frequency standards are performed by using an analogous crossed atom–standing-wave configuration, but the atomic beam is in general not well collimated. Because of the spread of transverse velocities, typically of the order of several Doppler speeds $v_D = \Gamma \lambda_L$, the overall absorption or fluorescence line shape is greatly broadened by the Doppler effect. For sufficiently strong laser intensities the broad Doppler profile exhibits a dip, called the Lamb dip; this can be as narrow as the natural transition linewidth and is centered at the exact atom transition frequency ω_0, which then provides the required frequency standard. Even within this configuration, where the dipole force is quite small, light-force-induced line-center shifts may occur due to atomic distribution modifications by the radiation-pressure force.

Although high-precision optical spectroscopy represents a basic and widely explored technique, surprisingly enough not much work to assess the mechanical effects of light on high-precision spectroscopy has appeared to our knowledge. We recall, e.g., that the determination of some fundamental physical constants [8], the experimental verification of atomic and QED theories [9], and the implementation of secondary frequency standards in the optical and infrared domain [10] are just a few remarkable instances that can rely heavily on the high resolution of optical spectroscopy methods.

In this paper we develop a simple model that enables us to calculate the effects of *dipole* and *radiation-pressure* forces on the spectroscopic determination of energy separations. We examine a configuration in which an atomic beam crosses at right angle two counterpropagating light beams of parallel linear polarizations (lin ∥ lin) and we explicitly refer to both regimes of fluorescence and saturation spectroscopy. We loosely denote by *fluorescence* or *saturation* spectros-

copy a situation in which the atomic beam carries a spread of transverse velocities sufficiently smaller or larger, respectively, than the Doppler speed v_D. In particular, the model provides the means for recovering the redshift observed in [7] as well as for explaining a blueshift of the Lamb dip line center for a closed transition in a beam of ^{4}He atoms discussed in Sec. VII. In Sec. II we derive general expressions for the excited level population and for the mean radiative force exerted on atoms moving in a standing wave. In Secs. III A and III B we specialize these general forms to useful closed-form expressions for the two specific regimes at issue here. We present in Sec. IV a suitable Fokker-Planck equation to describe the evolution of the position and momentum distribution function of the atoms as they cross the standing-wave laser field. The fluorescence line-shape profiles and corresponding line-center shifts observed in both the fluorescence and saturation spectroscopy regimes are respectively derived in Secs. V and VI by solving the relevant Fokker-Planck equation in the limit of short interaction times. The physical interpretation of these results is also given in these last two sections. We finally devote Sec. VII to a detailed comparison of our theoretical predictions with the experimental results for the Lamb dip blueshift observed in an effusive beam of atomic helium. The main conclusions of the work are summarized in Sec. VIII.

II. BACKGROUND

We largely follow the work of Cohen-Tannoudji in this one section by adapting the general results of [11] to a high-precision spectroscopy situation. In particular, we extend these results by including a detailed derivation of suitable expressions for the light-induced force and population required in the following sections.

We consider a mobile atom whose internal motion is subject to the two-level approximation involving only a ground state $|g\rangle$ and an excited state $|e\rangle$ whose energy levels are separated by $\hbar\omega_0$. The atom is coupled to a monochromatic laser light field whose frequency is denoted by ω_L but whose spatial distribution is initially unspecified. The atom is also coupled to a quantum field that accounts for the effect of spontaneous emission. In a frame rotating at a frequency ω_L the total Hamiltonian in the dipole approximation can be written as

$$H_{pr}=\frac{\hat{\mathbf{p}}^2}{2m}+\hbar\omega_0\pi^\dagger\pi-\hat{\mathbf{d}}\cdot\hat{\mathbf{E}}_L(\hat{\mathbf{r}},t)+\hat{H}_V+\hat{H}_{AV}(\hat{\mathbf{r}}). \quad (1)$$

Here $\hat{\mathbf{r}}$ and $\hat{\mathbf{p}}$ are the position and momentum operators of the center of mass with total mass m while π and $\pi^\dagger$ are the lowering and raising operators characterizing the internal states of the atom. The third term describes the interaction between the atomic dipole and the laser electric field taken at the center of mass position and the last two terms represent the energy of the quantum radiation field as well as the atom–quantum field coupling.

The center of mass motion of the atom can be described by the Heisenberg equation of motion for the position and the momentum operators. The velocity of the center of mass is given by

$$\frac{d\hat{\mathbf{r}}}{dt}=-\frac{i}{\hbar}[\hat{\mathbf{r}},\hat{H}]=\frac{\hat{\mathbf{p}}}{m} \quad (2)$$

so that the force operator can be obtained from the Heisenberg equation for $\hat{\mathbf{p}}$ with the help of Eq. (1),

$$\hat{\mathbf{F}}(\hat{\mathbf{r}},t)=m\ddot{\hat{\mathbf{r}}}=\frac{d\hat{\mathbf{p}}}{dt}=-\frac{i}{\hbar}[\hat{\mathbf{p}},\hat{H}]=\boldsymbol{\nabla}[\hat{\mathbf{d}}\cdot\hat{\mathbf{E}}_L(\hat{\mathbf{r}},t)]-\boldsymbol{\nabla}\hat{H}_{AV}(\hat{\mathbf{r}}). \quad (3)$$

Adopting the *semiclassical* approximation, we now assume that the atomic wave packet is sufficiently well localized in position and momentum so as to make the quantum description of the atomic motion as close as possible to the classical one. The position and momentum operators can be replaced by c functions $\mathbf{r}$ and $\mathbf{p}$ with a well prescribed time dependence. For this approximation to hold [12] the single-photon recoil frequency $\epsilon_R=\hbar k_L^2/2m$ must be appreciably smaller than the natural width Γ of the transition, i.e.,

$$\epsilon_R<\Gamma. \quad (4)$$

Further consideration of interaction times τ, which are of the order of the characteristic damping time ϵ_R^{-1} of the atomic velocity but longer than the radiative lifetime Γ^{-1} of the excited state, i.e.,

$$\Gamma^{-1}<\tau\lesssim\epsilon_R^{-1}, \quad (5)$$

enables one to deal with small variations of the external degrees of freedom of the atom (atomic position and momentum) after the internal ones have reached equilibrium.

We now give within this approximation the semiclassical expression for the mean radiative force experienced by the atom wave packet as it moves in a light field. If we take the quantum field initially in a vacuum state the last term on the right hand side of Eq. (3) vanishes upon averaging. On the other hand, by using the expression

$$\hat{\mathbf{d}}=\mathbf{d}(|e\rangle\langle g|+|g\rangle\langle e|) \quad (6)$$

for the dipole operator, where $\mathbf{d}=\mathbf{d}_{eg}=\mathbf{d}_{ge}$ is the dipole matrix element for the transition, and neglecting the antiresonant term, averaging over the first term on the right hand side of Eq. (3) can be carried out with the help of the general expression

$$\mathbf{E}_L(\mathbf{r},t)=\mathbf{e}_L\mathcal{E}_L(\mathbf{r})\cos[\omega_L t-\Phi(\mathbf{r})], \quad (7)$$

for the laser electric field. The laser is assumed to be in a coherent state where $\mathbf{e}_L$, $\mathcal{E}_L(\mathbf{r})$, and $\Phi(\mathbf{r})$ denote, respectively, its polarization, amplitude, and phase at $\mathbf{r}$ and are all taken to be real. Further averaging over the internal states of the atom leads to the general form of the mean radiative force [11]

$$\mathbf{F}(\mathbf{r},t) = -u(t)\boldsymbol{\nabla}_{\mathbf{r}}\hbar\Omega_1(\mathbf{r}) - v(t)\hbar\Omega_1(\mathbf{r})\boldsymbol{\nabla}_{\mathbf{r}}\Phi(\mathbf{r}). \quad (8)$$

Here we introduce the Rabi frequency as

$$\hbar\Omega_1(\mathbf{r}) = -\mathbf{d}\cdot\mathbf{e}_L\mathcal{E}_L(\mathbf{r}), \quad (9)$$

and the three independent components of the Bloch vector u, v, and w in terms of the reduced atomic density matrix elements ρ,

$$u(t) = \mathrm{Re}[\tilde{\rho}_{ge}(t)e^{-i\Phi(\mathbf{r})}], \quad (10)$$

$$v(t) = \mathrm{Im}[\tilde{\rho}_{ge}(t)e^{-i\Phi(\mathbf{r})}], \quad (11)$$

$$w(t) = \tfrac{1}{2}[\rho_{ee}(t) - \rho_{gg}(t)], \quad (12)$$

where g and e refer to the ground and excited states and the tilde to slowly varying matrix elements. The Bloch vector components (10)–(12) are found as solutions of the optical Bloch equations specific to the physical situation at issue.

In the present work we examine the case of an atomic beam propagating in the y direction, crossing a standing-wave laser field in the x direction ($\mathbf{k}_L = k_L\mathbf{x}$) and linearly polarized along z (lin $\|$ lin configuration). The mean force (8) then reduces to

$$\mathbf{F}(x,t) = -2\mathbf{k}_L\mathbf{d}\cdot\mathcal{E}_0\sin(k_Lx)u(t) \quad (13)$$

[$\Phi(\mathbf{r}) = 0$] and the relevant optical Bloch equations can be written in the matrix form,

$$\frac{d}{dt}\begin{pmatrix} u \\ v \\ w \end{pmatrix} = \begin{pmatrix} -\frac{\Gamma}{2} & \delta_L & 0 \\ -\delta_L & -\frac{\Gamma}{2} & -\Omega_1(x) \\ 0 & \Omega_1(x) & -\Gamma \end{pmatrix}\begin{pmatrix} u \\ v \\ w \end{pmatrix} - \begin{pmatrix} 0 \\ 0 \\ \frac{\Gamma}{2} \end{pmatrix}. \quad (14)$$

Here $\delta_L = \omega_L - \omega_0$, $\Omega_1(x) = -2\mathbf{d}\cdot\mathcal{E}_0\cos(k_Lx)/\hbar$ with $\mathcal{E}_0 = \mathbf{e}_L\mathcal{E}_L$, $\mathcal{E}_L$ being the real and constant amplitude of each counterpropagating component forming the standing wave. Because we take spatial variations of the laser standing wave to occur only along x, the y and z components of the atom velocity are here constant in time while the atomic motion in these two directions does not affect the evolution of its internal state. In Eqs. (13) and (14) the center of mass position is a prescribed function of time so that u, v, and w do depend on time also through the atom transverse trajectory $x = x(t)$.

If in Eq. (14) we denote by $X = (u,v,w)^T$ the Bloch vector, since we are restricted to interaction times longer than Γ^{-1} after which the $\partial X/\partial t$ contribution vanishes, we can rewrite the left hand side of Eq. (14) in terms of its hydrodynamics component only. In the case of uniform motion $x = v_xt$, with $v_x \simeq$ const, Eq. (14) reduces to a set of coupled differential equations whose coefficients are periodic in time and which we rewrite in the compact form,

$$v_x\frac{\partial X(x,v_x)}{\partial x} = \mathbf{B}(x)X(x,v_x) - X_S. \quad (15)$$

Here $\mathbf{B}(x)$ and X_S denote, respectively, the Bloch matrix and the source term on the right hand side of Eq. (14). The time dependence of x is here left implicit. The approximation of uniform motion is valid provided the transverse acceleration starts to become effective only over a time scale that is longer than the characteristic evolution times of the internal degrees of freedom of the atom.

Solutions of the modified form (15) of the optical Bloch equations give the time evolution of the atomic internal state for our specific atom-laser configuration; $X_3(t)$, in particular, yields the excited state instantaneous population $P_e(t)$ so that the corresponding fluorescence rate is

$$\phi(t) = \Gamma P_e(t) = \Gamma(\tfrac{1}{2} + X_3(t)). \quad (16)$$

III. FORCE AND POPULATION

A. Low-velocity expansions

We start this section by deriving an expression for the radiative force suitable for atoms moving with a velocity v_x along the laser standing-wave direction much smaller than the Doppler velocity $v_D = \Gamma\lambda\!\!\!^{-}_L$. Because in a time interval of the order of the excited level lifetime the atoms cross a distance v_x/Γ that is much smaller than a reduced wavelength $\lambda\!\!\!^{-}$, the internal state is essentially the steady state determined by the local optical potential created by the standing wave. Because most atoms will not have enough transverse kinetic energy to escape the periodic optical potential, this specific form of the force will be amenable to description as atomic fluorescence in trapping optical potentials of various standing-wave configurations [13].

We look for a perturbative solution of the modified optical Bloch equation (15) by expanding the Bloch vector in powers of v_x, i.e.,

$$X(x,v_x) = X^{(0)}(x) + v_xX^{(1)}(x) + v_x^2X^{(2)}(x) + \cdots, \quad (17)$$

where the coefficients have their usual meaning, i.e., $X^{(1)}(x) = \partial X(x,v_x)/\partial v_x$, $X^{(2)}(x) = \partial^2X(x,v_x)/\partial^2 v_x$, all evaluated at $v_x = 0$. Inserting this back into Eq. (15) and equating terms of the same power one easily arrives at the recursion relation

$$X^{(n)}(x) = \mathbf{B}^{-1}(x)\frac{\partial X^{(n-1)}(x)}{\partial x} \quad (n>1) \quad (18)$$

with the boundary condition

$$X^{(0)}(x) = \mathbf{B}(x)^{-1}X_S, \quad (19)$$

which represents the steady-state solution. With the help of Eqs. (18) and (19) we can evaluate the leading and first order contributions to the upper component u of $X(x,v_x)$ in Eq. (17) with which we derive in turn an approximated expression for the force (13) that is valid for very small values of v_x/v_D,

$$\mathbf{F}(x,v_x) = \mathbf{F}^{(0)}(x) + \mathbf{F}^{(1)}(x,v_x) + \cdots, \quad (20)$$

where

$$\mathbf{F}^{(0)}(x)=\hbar\mathbf{k}_L\Gamma\frac{2\delta_L S_R\sin 2k_Lx}{1+4S_R\cos^2 k_Lx}=-\boldsymbol{\nabla}_x\left(\frac{\hbar\delta_L}{2}\ln(1+4S_R\cos^2 k_Lx)\right) \tag{21}$$

and

$$\mathbf{F}^{(1)}(x,v_x)=\hbar\mathbf{k}_L\delta_L\frac{v_x}{v_D}16S_R\sin^2 k_Lx\frac{[\Gamma^2/(\Gamma^2+4\delta_L^2)](1-4S_R\cos^2 k_Lx)-8S_R^2\cos^4 k_Lx}{(1+4S_R\cos^2 k_Lx)^3}. \tag{22}$$

The saturation parameter is here defined as

$$S_R=\frac{2}{\Gamma^2+4\delta_L^2}\left(\frac{\mathbf{d}\cdot\mathcal{E}_0}{\hbar}\right)^2\equiv\frac{2}{\Gamma^2+4\delta_L^2}\Omega_0^2 \tag{23}$$

in terms of the single-beam Rabi frequency Ω_0. In a similar manner, we can evaluate the leading and first order contributions to the lower component w of $X(x,v_x)$ in Eq. (17), so that the corresponding expression for the upper level population again valid for very small v_x/v_D is

$$P_e(x,v_x)=P_e^{(0)}(x)+P_e^{(1)}(x,v_x)+\cdots \tag{24}$$

with

$$P_e^{(0)}(x)=\frac{1}{2}+X_3^{(0)}(x)=\frac{2S_R\cos^2 k_Lx}{1+4S_R\cos^2 k_Lx} \tag{25}$$

and

$$\begin{aligned}P_e^{(1)}(x,v_x)&=X_3^{(1)}(x,v_x)\\&=4\frac{v_x}{v_D}\frac{S_R\sin 2k_Lx}{(1+4S_R\cos^2 k_Lx)^3}\\&\quad\times\left(\frac{\Gamma^2}{\Gamma^2+4\delta_L^2}-\frac{\Gamma^2-4\delta_L^2}{\Gamma^2+4\delta_L^2}2S_R\cos^2 k_Lx\right).\end{aligned} \tag{26}$$

The results (20) and (24), which are *perturbative* in the atom transverse velocity but *exact* in the laser intensity, will be used at length in the following.

The zero-order terms represent the adiabatic solutions, valid when the atom is drifting so slowly along the standing-wave axis that its internal state, when it passes into x, is the same as that of an atom at rest in x. In particular, the force $F^{(0)}$ is purely *reactive* as it derives from the potential on the right hand side of Eq. (21) and physically it originates from the intensity gradient of the standing-wave profile.

The first order terms (22) and (26), on the other hand, are the leading order corrections to the force and population due to the motion of the induced atomic dipole in the spatially varying field intensity. The contribution $F^{(1)}$, in particular, is *dissipative* in nature as it depends also on the atom transverse velocity v_x. Notice that $F^{(1)}$, when averaged over a wavelength, takes the form of a ''friction'' force producing cooling or heating. In the limit of small saturations S_R's and negative (positive) detunings, Eq. (22) describes the well known *Doppler* cooling (heating) mechanism [14], while in the reverse limit of sufficiently high saturations and positive (negative) detunings the same force (22) describes the *Sysiphus* cooling (heating) mechanism [15].

B. All velocities expansions

We derive next an expression for the mean radiative force which is not restricted to small velocities as in the previous section. Such an expression can be obtained from a space average of the general form (13). For velocities v_x appreciably larger than the optical potential escape threshold, which is typically of the order of a fraction of v_D, the atoms will now have enough transverse kinetic energy to overcome the optical potential undisturbed. This specific form of the force will then be adequate for the description of atomic fluorescence in a saturation spectroscopy regime where the transverse spread of atomic velocities is larger than the characteristic value v_D.

The procedure is far more complicated than the one in the previous section and it will therefore be presented in some detail. Since the evolution matrix $\mathbf{B}(x)$ is periodic along x we look for a periodic steady-state solution of Eq. (15) in the form (Floquet theorem) [16]

$$X(x,v_x)=\sum_{n=-\infty}^{\infty}X^{(n)}(v_x)e^{ink_Lx}. \tag{27}$$

We consider again nearly uniform transverse motion $x=v_xt$ ($v_x\simeq$const). The complex vector $X^{(n)}(v_x)$ satisfies the property

$$X^{(n)}(v_x)^*=X^{(-n)}(v_x) \tag{28}$$

owing to the fact that all components of X are real. When the upper component of $X(x,v_x)$ in Eq. (27) is inserted into Eq. (13) the mean force averaged over a wavelength becomes with the help of Eq. (28)

$$\begin{aligned}\mathbf{F}(v_x)&=\langle\mathbf{F}(x,v_x)\rangle_{\lambda_L}\\&=-2\hbar\mathbf{k}_L\Omega_0\sum_{n=-\infty}^{\infty}\mathrm{Im}(X_1^{(n)}(v_x)\langle e^{ik_Lx(n+1)}\rangle)\\&=2\hbar\mathbf{k}_L\Omega_0\,\mathrm{Im}[X_1^{(1)}(v_x)],\end{aligned} \tag{29}$$

and similarly one has for the population

$$P_e(v_x)=\tfrac{1}{2}+\langle X_3(x,v_x)\rangle_{\lambda_L}$$
$$=\tfrac{1}{2}+\sum_{n=-\infty}^{\infty}X_3^{(n)}(v_x)\langle e^{ik_Lxn}\rangle$$
$$=\tfrac{1}{2}+X_3^{(0)}(v_x). \tag{30}$$

The Fourier components $X^{(n)}(v_x)$ are obtained from Eq. (18). After decomposing the trigonometric terms of $\mathbf{B}$ into a sum of two complex exponentials, the substitution of the trial solution (27) into Eq. (18) leads to the three-term recurrence relation

$$\mathbf{B}_1X^{(n-1)}+(\mathbf{B}_0-ik_Lv_xn)X^{(n)}+\mathbf{B}_1X^{(n+1)}=X_S\delta_{n,0}, \tag{31}$$

where

$$\mathbf{B}_0=\begin{pmatrix}-\Gamma/2 & \delta_L & 0\\ -\delta_L & -\Gamma/2 & 0\\ 0 & 0 & -\Gamma\end{pmatrix} \tag{32}$$

and

$$\mathbf{B}_1=\begin{pmatrix}0 & 0 & 0\\ 0 & 0 & \Omega_0\\ 0 & -\Omega_0 & 0\end{pmatrix}. \tag{33}$$

With the help of the ansatz

$$X^{(n)}=\mathbf{H}_{(n-1)}X^{(n-1)}+\tau_n, \tag{34}$$

Eq. (31) yields, for $n=0$, an equation for $X^{(0)}$ in the form

$$X^{(0)}=(\mathbf{B}_1\mathbf{H}_0^*+\mathbf{B}_1\mathbf{H}_0+\mathbf{B}_0)^{-1}(X_S-\mathbf{B}_1\tau_1^*-\mathbf{B}_1\tau_1) \tag{35}$$

and, for $n\geqslant 1$, equations for $\mathbf{H}_{n-1}$ and τ_n,

$$\mathbf{H}_{n-1}=(ik_Lv_xn-\mathbf{B}_0-\mathbf{B}_1\mathbf{H}_n)^{-1}\mathbf{B}_1, \tag{36}$$

$$\tau_n=(ik_Lv_xn-\mathbf{B}_0-\mathbf{B}_1\mathbf{H}_n)^{-1}\mathbf{B}_1\tau_{n+1}. \tag{37}$$

We omitted for simplicity the various functional dependences in the above matrix equations. We next assume that the $X^{(n)}$'s vanish for sufficiently large values of n so that $X^{(n_c)}=0$ after some cutoff value n_c, and from Eq. (34) one has $\tau_{n_c}=0$ and $\mathbf{H}_{n_c-1}=0$. This implies that when Eq. (36) is iterated down from n_c-1 to $n=1$ a matrix continued fraction solution for $\mathbf{H}_0$ can be found. Such a solution is rapidly converging and its explicit expression is given in Appendix A.

This step permits one to evaluate $\mathbf{H}_1,\mathbf{H}_2,\ldots,\mathbf{H}_{n_c-2}$ from Eq. (36) as well as X^0 from Eq. (35). When the same iteration procedure is applied to Eq. (37) one can show instead that the τ_n's are all vanishing for n spanning from n_c down to $n=1$ so that all Fourier coefficients $X^{(n)}$ can finally be evaluated through Eq. (34).

The position-averaged mean radiative force (29) then becomes

$$\mathbf{F}(v_x)=-2\hbar\Gamma\mathbf{k}_L\frac{\delta_L\Omega_0/\Gamma^2}{1+4(v_x/v_D)^2}$$
$$\times\frac{\mathrm{Im}(\mathbf{H}_0^{(2,3)})-2(v_x/v_D)\mathrm{Re}(\mathbf{H}_0^{(2,3)})}{1+2(\Omega_0/\Gamma)\mathrm{Re}(\mathbf{H}_0^{(2,3)})}, \tag{38}$$

whose leading order, e.g., is obtained by taking only the p_0 term in the continued fractions expansion (A1), that is,

$$\mathbf{F}^{(0)}(v_x)=\hbar\Gamma\mathbf{k}_L\frac{\delta_L(k_Lv_x)}{\Gamma^2+4\delta_L^2}$$
$$\times\frac{8S_R}{(1+2S_D)(1+2S_D+2S_R)-16S_DS_{\delta_L}}. \tag{39}$$

Similarly one has for the excited level population

$$P_e(v_x)=\frac{\Omega_0}{\Gamma}\frac{\mathrm{Re}(\mathbf{H}_0^{(2,3)})}{1+2(\Omega_0/\Gamma)\mathrm{Re}(\mathbf{H}_0^{(2,3)})}, \tag{40}$$

whose leading order reads as

$$P_e^{(0)}(v_x)=\frac{S_R(1+2S_D)}{(1+2S_D)(1+2S_D+2S_R)-16S_DS_\delta}. \tag{41}$$

As in Eq. (23) we introduce the parameters,

$$S_D=2\frac{(k_Lv_x)^2}{\Gamma^2+4\delta_L^2},\quad S_{\delta_L}=2\frac{\delta_L^2}{\Gamma^2+4\delta_L^2}. \tag{42}$$

Unlike the results (20) and (24), which are valid for small transverse velocities, the expressions for the force (38) and the population (40) hold for *all* transverse velocities, though the number of required terms in the fraction form of $\mathbf{H}_0$ grows with increasing intensities. In particular, the leading order terms (39) and (41) are valid for moderate intensities. We find in fact that when $\Omega_0/\Gamma\lesssim 2$ no substantial changes in the force or population are observed by including the higher-order terms $p_1,p_2,p_3,\ldots$ in the fraction expansion (A1).

Such terms, on the other hand, are required when higher laser intensities are involved. At intensities as high as $\Omega_0/\Gamma=8$, e.g., it can be seen that both force and population profiles start to become indistinguishable only beyond the fourth (or higher) order term. At these intensities the four terms p_1, p_2, p_3, and p_4 need to be included for the expansion (A1) to converge.

IV. FLUORESCENCE LINE SHAPE

For atoms moving in a light field the optical Bloch equations (14) and (15) should be generalized to the case where the atom external degrees of freedom (position and momentum) are taken into account. Yet, based on the adiabatic separation Eq. (4) between the (fast) internal degrees of freedom, which vary on a time scale of $\sim\Gamma^{-1}$, and the (slow) external

ones, which vary on a time scale of $\sim\epsilon_R^{-1}$, the master equation for ρ can be recast into an equation that includes only external variables. This is commonly achieved by writing the master equation for ρ in a mixed position-momentum (Wigner) representation where ρ is described by a matrix $W(\mathbf{r},\mathbf{p},t)$, and then tracing W over the internal variables.

Such a trace defines the atomic distribution function $f(\mathbf{r},\mathbf{p},t)$ which represents in essence the probability for finding an atom at $\mathbf{r}$ and at time t moving with momentum $\mathbf{p}$, regardless of its internal state. Either for slow atoms ($v_x \lesssim v_D$) in any laser light field [12] or for faster ones ($v_x > v_D$) in a standing-wave light field [17], the evolution of the distribution function f can be described by a Fokker-Planck type of equation which reads for both situations as

$$\frac{\partial f}{\partial t} = -\frac{p_x}{m}\frac{\partial f}{\partial x} - \frac{p_y}{m}\frac{\partial f}{\partial y} - \frac{\partial [F_x f]}{\partial p_x} + \sum_{i,j=\{x,y,z\}} \mathcal{D}_{i,j}\frac{\partial^2 f}{\partial p_i \partial p_j}. \tag{43}$$

The first two contributions on the right hand side are hydrodynamic terms describing the free spatial evolution of the distribution function, given its velocity. The next one describes the drift in momentum of the distribution function due to the *mean* radiative force, which accounts here for either its conservative or dissipative component. The last contribution describes instead effects of momentum *diffusion* originating from fluctuations in the momentum carried away by spontaneously emitted photons and fluctuations in momentum exchanges between the atom and the driving laser field.

Because we restrict ourselves to interaction times τ of several atomic lifetimes and not much longer than ϵ_R^{-1} [see Eq. (5)], we can neglect to a very good approximation the effect of diffusion due to either spontaneous emission or to the random character of the momentum exchange between the atom and the field. Stationary solutions of the modified Fokker-Planck equation

$$\bar{v}_{\bar{y}}\frac{\partial f(\bar{x},\bar{y},\bar{v}_{\bar{x}})}{\partial \bar{y}} + \bar{v}_{\bar{x}}\frac{\partial f(\bar{x},\bar{y},\bar{v}_{\bar{x}})}{\partial \bar{x}} = -2\bar{\epsilon}_R\frac{\partial [\bar{F}_{\bar{x}}(\bar{x},\bar{v}_{\bar{x}})f(\bar{x},\bar{y},\bar{v}_{\bar{x}})]}{\partial \bar{v}_{\bar{x}}}, \tag{44}$$

subject to the initial condition

$$f(\bar{x},\bar{y}=0,\bar{v}_{\bar{x}}) = \frac{1}{\bar{\sigma}\sqrt{2\pi}}\exp(-\bar{v}_x^2/2\bar{\sigma}^2), \tag{45}$$

will then be needed in the following. We introduce the dimensionless variables

$$\bar{x} = k_L x, \quad \bar{v}_x = v_x/v_D, \quad \bar{F}_x = F_x/\hbar k_L \Gamma, \tag{46}$$

and a similar scaling holds for $\bar{y}$, $\bar{v}_y$, and $\bar{\sigma}$. The condition (45) represents an initial distribution that is uniform in space but exhibits a Gaussian velocity profile with transverse mean spread $\bar{\sigma}$. The ratio

TABLE I. Numerical values of the scaled recoil frequency $\bar{\epsilon}_R$ and the relevant atomic transition.

Atom	Transition	$\bar{\epsilon}_R$
^{1}H	$1\,^2S_{1/2}-2\,^2P_{3/2}$	0.135
^{4}He	$2\,^3S_1-2\,^3P_2$	0.025
^{7}Li	$2\,^2S_{1/2}-2\,^2P_{3/2}$	0.010
^{23}Na	$3\,^2S_{1/2}-3\,^2P_{3/2}$	0.0025
^{39}K	$4\,^2S_{1/2}-4\,^2P_{3/2}$	0.0014
^{133}Cs	$6\,^2S_{1/2}-6\,^2P_{3/2}$	4.1×10^{-4}

$$\bar{\epsilon}_R = \epsilon_R/\Gamma = \hbar k_L^2/2m\Gamma \tag{47}$$

between the characteristic times of the internal and translational degrees of freedom provides a measure of the coupling strength between them. For most atomic transitions, $\bar{\epsilon}_R$ is quite low and values for some cases of experimental interest [13] are given in Table I. Since we take the light field here to have a uniform longitudinal profile we omit the y dependence of the force in the evolution equation (44). All atoms are then assumed to travel along y with the same constant velocity v_y. Likewise for the force z dependence, in which case we take $v_z = 0$.

We specifically investigate two regimes that occur in fluorescence spectroscopy and saturation spectroscopy experiments: the former and the latter refer, respectively, to an incident atomic beam whose transverse velocity spread is much smaller ($\bar{\sigma} \ll 1$) or much larger ($\bar{\sigma} \gg 1$) than the characteristic velocity v_D. The prototype experiment which we examine in the following consists in collecting the fluorescence from an ensemble of atoms as they move a distance d across the uniform longitudinal profile of the laser. The observable of interest is the corresponding rate of fluorescence emitted per solid angle by the atoms. This yields the fluorescence line shape and is directly proportional to the population average $\langle P_e(\ldots)\rangle$ obtained by integrating over the initial transverse velocity and all positions, i.e.,

$$\Phi = \frac{1}{\mathcal{N}}\int_{-\infty}^{\infty} d\bar{v}_x \int_0^{2\pi} d\bar{x} \int_0^{\bar{d}} d\bar{y}\, P_e(\bar{x},\bar{v}_x) f(\bar{x},\bar{y},\bar{v}_x). \tag{48}$$

We denote here by $\mathcal{N}$ the usual normalization factor for the distribution f.

When mechanical effects are absent the distribution f will maintain its initial form (45): this is a solution of the Fokker-Planck equation (44) with $\bar{F}_x = 0$, or in the limiting case of a very heavy atom ($m \to \infty$). The corresponding line-shape profile Φ can easily be evaluated from Eq. (48) with the help of Eq. (45) and the appropriate leading order contribution to the upper level population, i.e., $P_e^{(0)}$ in Eq. (25) or $P_e^{(0)}$ in Eq. (41), respectively, for a beam carrying a small or a large spread $\bar{\sigma}$. The line-shape profiles are shown in Fig. 1 for both cases: in the fluorescence spectroscopy regime ($\bar{\sigma} \ll 1$) one has a *peak* centered at the atom transition frequency while in the saturation spectroscopy regime ($\bar{\sigma} \gg 1$) one has a *dip* at

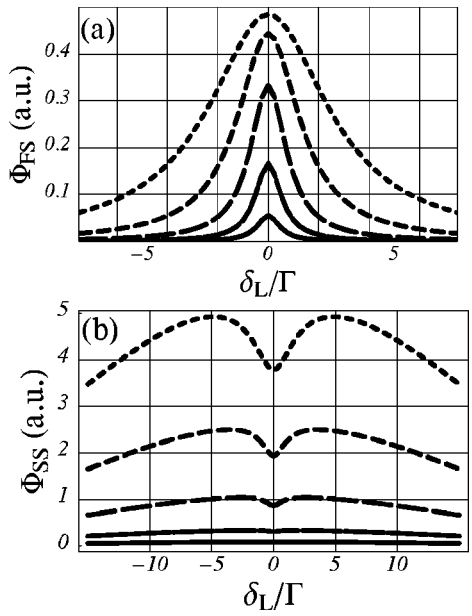

FIG. 1. Typical fluorescence signal in the absence of mechanical effects of light. Frames (a) and (b) refer, respectively, to a transverse velocity spread of $\sigma=10^{-2}v_D$ and $\sigma=15v_D$. In each frame the intensity increases from the bottom up with $\Omega_0/\Gamma=0.12$, 0.25, 0.5, 1, 2.

the same position. Owing to the usual power broadening of a saturable absorber both profiles broaden as the intensity increases.

When mechanical effects are taken into account the derivation of the fluorescence line-shape profile is not straighforward owing to the complicated modification of the distribution function f over the width d. On one hand, atoms from a beam with a narrow spread $\bar{\sigma}$ will be essentially affected by a (conservative) force that is periodic in space. One then expects a spatially modulated atomic distribution function. On the other hand, atoms from a beam with a broad spread $\bar{\sigma}$ will move undisturbed across the optical potential but will experience an averaged (dissipative) force that leads to either cooling or heating as discussed earlier in Sec. II. In this case the atomic distribution function will remain nearly uniform in space while momentum focusing (cooling) or defocusing (heating) effects will introduce an increase or a decrease in the number of slow atoms.

In the next two sections we will examine these two cases in some detail.

V. FLUORESCENCE SPECTROSCOPY REGIME: LINE-SHAPE MODIFICATIONS

In this section we examine the case in which the incident atoms carry very small mean spread of transverse velocities ($\bar{\sigma}\ll 1$). One expects that most of the atoms will not have enough (transverse) kinetic energy to escape the optical potential. For appropriately short interaction times $\tau=y/v_y$ mechanical effects will not much alter the initial distribution of atomic position and momenta. Upon the change of variable $\bar{y}\to\Gamma\tau=\bar{\tau}$, we can then expand f around $\bar{\tau}=0$,

$$f_{FS}(\bar{x},\bar{\tau},\bar{v}_x)=f^{(0)}(\bar{x},\bar{v}_x)+\bar{\tau}f^{(1)}(\bar{x},\bar{v}_x)+\frac{\bar{\tau}^2}{2}f^{(2)}(\bar{x},\bar{v}_x)+\cdots, \tag{49}$$

where the coefficients $f^{(0)},f^{(1)},f^{(2)},\ldots$ have their usual meaning. By inserting Eq. (49) into Eq. (44) one obtains the following recursion relation for the coefficients ($n\geqslant 1$):

$$f^{(n)}(\bar{x},\bar{v}_x)=-\left(\bar{v}_x\frac{\partial}{\partial\bar{x}}+2\bar{\epsilon}_R\bar{F}_x(\bar{x})\frac{\partial}{\partial\bar{v}_x}\right)f^{(n-1)}(\bar{x},\bar{v}_x). \tag{50}$$

The initial distribution (45) is spatially uniform and the first two coefficients can be written as

$$f^{(1)}(\bar{x},\bar{v}_x)=-2\bar{\epsilon}_R\bar{F}_x(\bar{x})\frac{\partial}{\partial\bar{v}_x}f^{(0)}(\bar{v}_x) \tag{51}$$

and

$$f^{(2)}(\bar{x},\bar{v}_x)=\left(4\bar{\epsilon}_R^2\bar{F}_x^2(\bar{x})\frac{\partial^2}{\partial\bar{v}_x^2}\right)f^{(0)}(\bar{v}_x)+\left(2\bar{\epsilon}_R\bar{v}_x\frac{\partial\bar{F}_x(\bar{x})}{\partial\bar{x}}\frac{\partial}{\partial\bar{v}_x}\right)f^{(0)}(\bar{v}_x), \tag{52}$$

where $\bar{F}_x$ is here the force zero-order contribution (21) appropriate for the case of small transverse velocities. These results, along with the population zero-order contribution (25), are now used to derive an expression for the fluorescence linewidth Φ. The first order contribution (51) and the first term of the second order contribution (52) vanish upon velocity averaging. After a lengthy position and velocity averaging procedure one obtains from Eq. (48)

$$\begin{aligned}\Phi_{FS}&\simeq\Phi_{FS}^{(0)}+\Phi_{FS}^{(2)}\\&=\frac{1}{\mathcal{N}_{FS}}\int_0^{2\pi}d\bar{x}\,P_e(\bar{x})\\&\quad\times\int_{-\infty}^{\infty}d\bar{v}_x\left(f^{(0)}(\bar{v}_x)+\frac{(\Gamma\tau_0)^2}{6}f^{(2)}(\bar{x},\bar{v}_x)\right)\\&=\frac{\pi}{\mathcal{N}_{FS}}\left[\left(1-\frac{1}{\sqrt{1+4S_R}}\right)-\epsilon_R\tau_0^2\frac{8\delta_L S_R^2}{(1+4S_R)^{3/2}}\right].\end{aligned} \tag{53}$$

We denote here by τ_0 the traversal time d/v_y. The two separate contributions $\Phi_{FS}^{(0)}$ and $\Phi_{FS}^{(2)}$ as well as the entire fluorescence profile Φ_{FS} are shown in Fig. 2. The lowest order correction $\Phi_{FS}^{(2)}$ is proportional to $\epsilon_R\tau_0^2$, i.e., to the square of the traversal time and to the inverse of the atomic mass; as expected, the larger the mass the smaller the correction. The perturbative approach is then valid for sufficiently small values of this product. For ^{4}He atoms ($\bar{\epsilon}_R=0.025$), the traversal time should not exceed several radiative lifetimes; longer times are likely, however, for heavier alkali-metal atoms (see Table I).

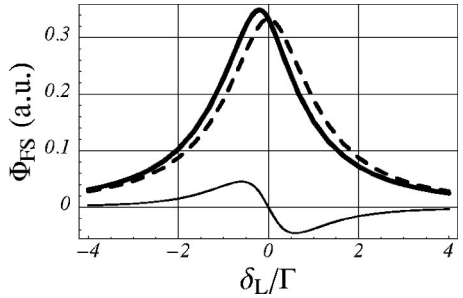

FIG. 2. Typical fluorescence signal including mechanical effects of light (fluorescence spectroscopy regime) for $\tau_0=0$ (dashed) and $\tau_0=(0.25\bar{\epsilon}_R^{-1})^{1/2}\Gamma^{-1}$ (solid) and $\Omega_0/\Gamma=1$. The thin curve at the bottom corresponds to their difference.

The leading term $\Phi_{FS}^{(0)}$, when the explicit expression for S_R is substituted into it, describes a Lorenztian-like fluorescence profile which is symmetric with detuning. It yields the spectra in the absence of mechanical effects shown in Fig. 1(a). The correction $\Phi_{FS}^{(2)}$ is instead asymmetric with respect to δ_L and it is responsible for line-shape asymmetries; for red (blue) detunings it gives rise to a small increase (decrease) of the fluorescence, acquiring the maximum value

$$\Phi_{FS}^{(2),\max}=(\Omega_0\tau_0)^2\frac{6\sqrt{3}\epsilon_R\Omega_0^2}{\Gamma^3+9\Gamma\Omega_0^2+(\Gamma^2+6\Omega_0^2)^{3/2}} \tag{54}$$

at

$$\delta_L^{\max}=-\frac{\Gamma}{\sqrt{6}}\left[\left(1+6\frac{\Omega_0^2}{\Gamma^2}\right)^{1/2}-\frac{1}{2}\right]^{1/2}. \tag{55}$$

The increase (decrease) of the total fluorescence Φ for red (blue) detunings thus grows with the intensity and is proportional to the square of the interaction time. We display in Fig. 3(a) the redshift of the total fluorescence maximum as the intensity increases. These predictions all recover previous experimental observations of Prentiss and Ezekiel [7].

The shift originates from modifications of the atomic trajectory due to the transverse force on the atomic dipole in the field gradient of the standing wave. For atoms that experience no transverse force, such as very heavy ones, for example, there will be no modification of the initial distribution and line shape $\Phi_{FS}^{(0)}$. Atoms that experience the transverse force (21), on the other hand, are pushed toward high-intensity regions when the exciting field is detuned below resonance and toward zero-field-intensity regions when it is detuned above resonance. The second form of the force (21) clearly illustrates this mechanism. In this case, since the fluorescence rate is obviously higher for atoms located at high-field positions, the fluorescence profile $\Phi_{FS}^{(0)}$ will be modified by the asymmetric contribution $\Phi_{FS}^{(2)}$. Hence for traversal times (τ_0) and recoils (ϵ_R) small enough to be consistent with the perturbative expansion (49)–(53) and for $\delta_L<0$ ($\delta_L>0$), there will be atoms accumulating in the high-intensity (zero-intensity) regions of the wave, causing a fluorescence yield higher (lower) than that corresponding to an unmodified velocity distribution. This line-shape asymmetry is observable as a net line-center shift toward lower frequencies.

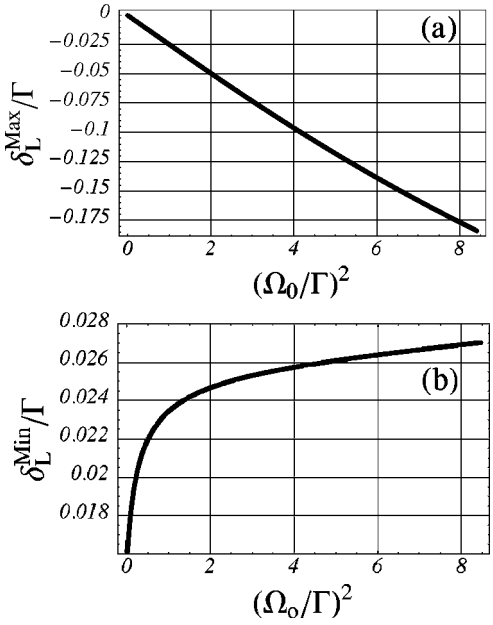

FIG. 3. Line-center shift vs intensity of the standing-wave laser field. (a) refers to the fluorescence spectroscopy regime with $\tau_0=(0.025\bar{\epsilon}_R^{-1})^{1/2}\Gamma^{-1}$. (b) refers to the saturation spectroscopy regime with $\tau_0=0.125\bar{\epsilon}_R^{-1}\Gamma^{-1}$. Here $\bar{\epsilon}_R=0.025$ as for the ^{4}He experiment described in Sec. VII.

VI. SATURATION SPECTROSCOPY REGIME: LINE-SHAPE MODIFICATIONS

In this section we proceed to examine the case of an incident beam with a wide spread of transverse velocities ($\bar{\sigma}\gg 1$). The atoms have in this case a transverse kinetic energy large enough to slide over the spatial variations of the optical potential and to be insensitive to the conservative component of the radiative force. The atomic distribution f will not exhibit a significant dependence on $\bar{x}$, which we neglect, i.e., $f(\bar{x},\bar{y},\bar{v}_x)\to f(\bar{\tau},\bar{v}_x)$. Upon performing the change of variable $\bar{y}\to\bar{\tau}$, as in the previuos section, the corresponding Fokker-Planck equation (44) will take on the simplified form

$$\frac{\partial}{\partial\bar{\tau}}f(\bar{\tau},\bar{v}_x)=-2\bar{\epsilon}_R\frac{\partial}{\partial\bar{v}_x}[\bar{F}_x(\bar{v}_x)f(\bar{\tau},\bar{v}_x)]. \tag{56}$$

For short interaction times $\bar{\tau}$ we can look again for a perturbative solution of Eq. (56) by expanding f in powers of $\epsilon_R\tau$ around $\bar{\tau}=0$,

$$f_{SS}(\bar{\tau},\bar{v}_x)=f^{(0)}(\bar{v}_x)+\bar{\tau}f^{(1)}(\bar{v}_x)+\frac{\bar{\tau}^2}{2!}f^{(2)}(\bar{v}_x)+\cdots \tag{57}$$

with $f^{(0)}(\bar{v}_x)$ given in Eq. (45). Upon inserting Eq. (57) into Eq. (56) we obtain the following recursion relation ($n\geqslant 1$):

$$f^{(n)}(\bar{v}_x) = -2\bar{\epsilon}_R \frac{\partial}{\partial \bar{v}_x}[\bar{F}_x(\bar{v}_x) f^{(n-1)}(\bar{v}_x)]. \tag{58}$$

Since the spread of velocities over which $P_e(\bar{v}_x)$ in Eq. (48) takes on nonvanishing values is much smaller than $\bar{\sigma}$, we can replace $f^{(0)}(\bar{v}_x)$ by the constant value $f^{(0)}(0)$ at $v_x = 0$. Thus the first and second order contributions become

$$f^{(1)}(\bar{v}_x) \simeq -2\bar{\epsilon}_R f^{(0)}(0) \frac{\partial}{\partial \bar{v}_x} \bar{F}_x(\bar{v}_x) \tag{59}$$

and

$$f^{(2)}(\bar{v}_x) \simeq 2\bar{\epsilon}_R^2 f^{(0)}(0) \frac{\partial^2 \bar{F}_x^2(\bar{v}_x)}{\partial \bar{v}_x^2}. \tag{60}$$

where $\bar{F}_x$ is the position-averaged mean force (39) that is appropriate for large values of the atomic transverse velocity and moderate intensities ($\Omega_0/\Gamma \lesssim 2$). As in Eq. (48) the fluorescence linewidth can in this case be written as

$$\begin{aligned} \Phi_{SS} &\simeq \Phi_{SS}^{(0)} + \Phi_{SS}^{(1)} \\ &= \frac{f^{(0)}(0)}{\mathcal{N}_{SS}} \int_{-\infty}^{\infty} d\bar{v}_x \, P_e(\bar{v}_x) - \epsilon_R \tau_0 \frac{f^{(0)}(0)}{\mathcal{N}_{SS}} \\ &\quad \times \int_{-\infty}^{\infty} d\bar{v}_x \, P_e(\bar{v}_x) \frac{\partial}{\partial \bar{v}_x} \bar{F}_x(\bar{v}_x), \end{aligned} \tag{61}$$

and comprises two terms. The lowest-order correction $\Phi_{SS}^{(1)}$, proportional to $\epsilon_R \tau_0$, grows linearly with the traversal time and with the inverse mass so that the perturbative approach used here is now valid for appropriately small values of the product $\epsilon_R \tau_0$.

The zeroth-order term $\Phi_{SS}^{(0)}$ depends on the laser detuning through the excited state population P_e which is even in δ_L and gives rise to a symmetric Lamb dip as shown in Fig. 1(b). The lowest correction $\Phi_{SS}^{(1)}$ depends on the detuning also through the force $\bar{F}_x$ which is instead odd with δ_L: this causes an asymmetry of the Lamb dip profile whose line center (minimum) becomes appreciably blueshifted from exact resonance. We report in Fig. 4 the evolution of the Lamb dip profile for increasing traversal times at fixed laser intensity. The change with time of the line center toward higher frequencies is nearly linear as shown in Fig. 5 for different intensities. We have verified the validity of our perturbative result (61) by checking the relative smallness of higher-order corrections. For ^{4}He atoms, $\bar{\epsilon}_R = 0.025$ (see Table I), we predict a shift of about 0.1Γ to occur over a traversal time $\tau_0 \simeq 20\Gamma^{-1}$ while the inclusion of the term $\Phi_{SS}^{(2)}$ (solid line) affects only slightly the contribution $\Phi_{SS}^{(1)}$ (dashed line), apart from a rather small saturation of the shift at longer times. We also examined the dependence of the line-center shift on the intensity, which we report in Fig. 3(b). As in the case of fluorescence spectroscopy the shift increases with the intensity.

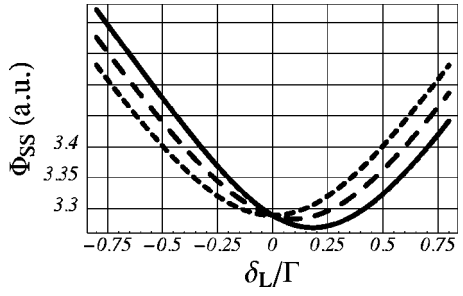

FIG. 4. Saturation spectroscopy regime: typical Lamb dip line-center enlargement including mechanical effects of light for $\tau_0 = 0$ (short dashed), $\tau_0 = (0.5\bar{\epsilon}_R^{-1})\Gamma^{-1}$ (long dashed), and $\tau_0 = (\bar{\epsilon}_R^{-1})\Gamma^{-1}$ (solid) and with $\Omega_0/\Gamma = 1.8$.

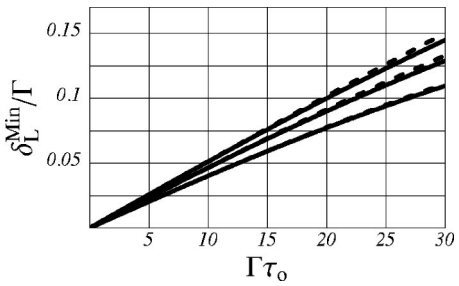

FIG. 5. Lamb dip line-center shift $\delta_L^{\min}$ vs traversal time τ_0 and intensities increasing from the bottom up with $\Omega_0/\Gamma = 0.5,1,2$. Here $\bar{\epsilon}_R = 0.025$ as for the ^{4}He experiment described in Sec. VII. We include leading orders in the expansion (61) up to $\Phi_{SS}^{(2)}$ (solid) and $\Phi_{SS}^{(1)}$ (dashed).

Such a shift of the Lamb dip line center has been recently observed for the *cycling* transition $2\,^3S_1 \rightarrow 2\,^3P_2$ in ^{4}He atoms; the relevant experimental results and comparison with the present theory are reported separately in the next section.

The physics underlying the line-center blueshift (Fig. 4) can be understood in the following way. When the laser is red detuned ($\delta_L < 0$) the atoms are Doppler cooled (*transverse cooling*); this increases the initial number of slow atoms, i.e., atoms with a velocity $v_x \lesssim v_D$, that contribute to the Lamb dip profile, so that a larger fluorescence yield, i.e., a rise in the Lamb dip low-frequency shoulder occurs with respect to the situation of an unmodified atomic distribution function. Conversely, when the laser field is blue detuned ($\delta_L > 0$) heating takes place so that the number of slow atoms decreases, with a subsequent lowering of the dip high-frequency shoulder. It is clear, upon combining these two effects, that the fluorescence yield increase (decrease) for red (blue) detunings produces a profile asymmetry responsible for the Lamb dip line-center shift toward the high-frequency region.

VII. EXPERIMENT

We present in this section the experimental observation of a blueshift of the sub-Doppler line-center dip occurring for a closed transition of helium in the crossed atom-laser configuration studied in the previous sections. In our experiment we shine laser light at 1083 nm, close to the $2\,^3S_1 \rightarrow 2\,^3P_2$ tran-

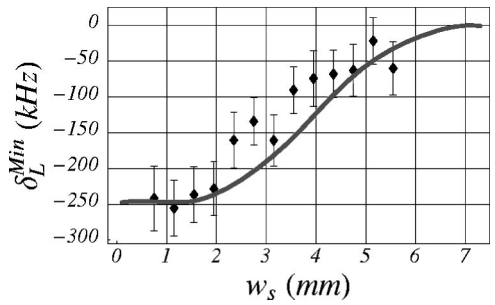

FIG. 6. Blueshift $\delta_L^{\min}$ of the sub-Doppler dip vs slit aperture w_S: experimental data (●) and theoretical predictions (solid line) derived after Eq. (63) for a peak intensity $I_0=0.6\times 14(1)\times I_{\rm sat}$. Line centers are measured with respect to the largest line-center shift obtained with an unobstructed laser beam (zero level).

sition, on a beam of metastable ^{4}He atoms excited to the $2\,^3S_1$ state by means of a dc discharge (50–100 V). The natural linewidth [full width at half maximum (FWHM)] of the transition is $\Gamma/2\pi=1.6$ MHz corresponding to a Doppler speed $v_D=\Gamma\lambda_L\simeq 1.7$ m/s. The laser frequency is measured with respect to a nearby frequency reference obtained by stabilizing a second laser on the saturated absorption signal of a helium cell discharge. We use for the purpose two semiconductor diode lasers in an extended cavity configuration (linewidth ~0.2 MHz). Unlike a gas cell, an atomic beam appears particularly favorable to the observation of a shift because collisions commonly hamper the modifications of the atomic momentum distribution and hence inhibit the shift [18].

The resonant laser beam (single beam power of 0.15 mW) is linearly polarized along the direction of flight of the atoms and retroreflected with the same polarization and intensity (lin ∥ lin). The transverse Doppler profile of the atomic beam is 120 MHz wide (FWHM) and we detect the sub-Doppler feature in the fluorescence signal by passing the atoms across such a standing-light-wave configuration. The emitted fluorescence is collected by a phototube placed above the laser-atom interaction region while the line-center shifts are measured for different values of the laser beam width d. This is done by means of a slit that chops the tail of the laser beam at different positions with a Gaussian profile and a beam radius $w_L=2.1(1)$ mm ($1/e^2$ intensity). The adjustable slit is followed by two positive lenses ($f=1$ m) on the ingoing beam plus a third positive lens ($f'=0.2$ m) on the retroreflected beam. The two f lenses are 2 m apart and 1 m away from both the adjustable slit and the interaction region. The third lens is placed midway between the interaction region and the retroreflecting mirror and 0.2 m away from both. This setup assures that the wave front is not distorted for either counterpropagating component and, in particular, it enables us to change the width of the laser beam without changing its peak intensity. A further detailed description of the experimental setup is deferred to [19].

Our measurements are performed by alternating each scan across resonance needed to obtain the dip profile for a given slit aperture w_S by another one taken with an unobstructed laser beam; we report in Fig. 6 the difference between the two recordings for increasing values of w_S. The second reading (fully open slit) sets a reference for each frequency measurement. A quantitative comparison between theory and experiment clearly relies on the appropriate relation between the effective duration τ of the interaction and the slit width w_S. Such a relation is affected mainly by the nonuniform distribution of longitudinal (atomic) velocities and by the fact that for sufficiently large slit apertures the atoms no longer experience a constant light intensity as they cross the beam. Thus modifications of the atomic distribution and the subsequent line-center shifts depend on the slit width in a rather complicated fashion. This may be examined by generalizing Eq. (57) to include a position-dependent force $\bar{F}_x$. Because the effective laser spot size w_S is much larger than the wavelength λ_L, the y and z components of the force are much smaller than the corresponding force along x and can both be neglected as was done in the theory. We formally integrate Eq. (56) between (any) two times τ_i and τ_f and then solve the resulting Fokker-Planck equation. Because in our experiment $\bar{\epsilon}_R/\bar{v}_y\sim 10^{-5}$ for intervals short enough so that $\bar{\epsilon}_R(\bar{\tau}_f-\bar{\tau}_i)\ll 1$, or for separations $(\bar{y}_f-\bar{y}_i)\ll \bar{v}_y/\bar{\epsilon}_R$, it is sufficient to proceed by iterations and retain the lowest order,

$$
\begin{aligned}
f(\bar{y}_f,\bar{v}_x,\bar{v}_y)&\simeq f(\bar{y}_i,\bar{v}_x,\bar{v}_y)\\
&\quad -2\frac{\bar{\epsilon}_R}{\bar{v}_y}\int_{\bar{y}_i}^{\bar{y}_f}\partial_{\bar{v}_x}[\bar{F}_x(\bar{y},\bar{v}_x)f(\bar{y}_i,\bar{v}_x,\bar{v}_y)]d\bar{y}\\
&\simeq f(\bar{y}_i,\bar{v}_x,\bar{v}_y)\left(1-2\frac{\bar{\epsilon}_R}{\bar{v}_y}\int_{\bar{y}_i}^{\bar{y}_f}\partial_{\bar{v}_x}\bar{F}_x(\bar{y},\bar{v}_x)d\bar{y}\right).
\end{aligned}
\tag{62}
$$

The approximation in the last step is always satisfied for a sufficiently wide initial distribution (45), which again conforms to our experimental situation as the initial spread $\bar{\sigma}\approx 10^2$. The rate of fluorescence emitted per solid angle is proportional to the average population, which is here obtained, as in Eq. (48), by integrating over both longitudinal and transverse velocities, and over a slit of width w_S,

$$
\begin{aligned}
\Phi_{SS}^{\rm expt}&=\frac{1}{\mathcal{N}_{SS}^{\rm expt}}\int_{-\bar{w}_S/2}^{\bar{w}_S/2}d\bar{y}\int_{-\infty}^{\infty}d\bar{v}_x\,P_e(\bar{y},\bar{v}_x)\\
&\quad\times\int_0^{\infty}d\bar{v}_y\,N(\bar{v}_y)f(\bar{y},\bar{v}_x,\bar{v}_y),
\end{aligned}
\tag{63}
$$

where

$$
f(\bar{y},\bar{v}_x,\bar{v}_y)=f(\bar{y}_0,\bar{v}_x,\bar{v}_y)\exp\left(-2\frac{\bar{\epsilon}_R}{\bar{v}_y}\partial_{\bar{v}_x}\int_{\bar{y}_0}^{\bar{y}}d\bar{y}'\bar{F}_x(\bar{y}',\bar{v}_x)\right)
\tag{64}
$$

is the atomic distribution at an arbitrary point $\bar{y}$ in terms of the distribution $f(\bar{y}_0,\bar{v}_x,\bar{v}_y)$ at some point $\bar{y}_0$. The result (64) can be derived through a limiting procedure that generalizes Eq. (62) and details are given in Appendix B.

We now proceed to evaluate Φ_{SS}^{expt} with the full distribution (64). For the moderate intensities of the experiment ($\Omega_0 \lesssim 2\Gamma$) we can replace the population in Eq. (63) and the force (64) by their lowest-order contributions (41) and (39), where the saturation S_R should in turn take the position-dependent form

$$S_R(\bar{y}) = \frac{I_{\text{peak}}/I_{\text{sat}}}{1+4(\delta_L/\Gamma)^2}\exp(-2\bar{y}^2/\bar{w}_L^2) \tag{65}$$

appropriate to a Gaussian laser beam of waist radius w_L. Here I_{peak} and I_{sat} denote, respectively, the peak value of the laser intensity and the effective saturation intensity. The distribution $N(v_y)$ of longitudinal velocities, on the other hand, has been inferred by measuring the Doppler profile of the fluorescence in a standard copropagating laser-atomic beam configuration. This turns out to be a generalized Maxwell distribution,

$$N(\bar{v}_y) = N_0(\bar{v}_y/\bar{u})^\beta \exp(-\bar{v}_y^2/\bar{u}^2), \tag{66}$$

with

$$\beta = 5.6(1) \quad \text{and} \quad \bar{u} = 0.93(2)\times 10^3, \tag{67}$$

and N_0 a suitable normalization constant. The most probable value of the distribution (66) is considerably larger than the thermal velocity of helium at 77 K mainly because electron collisions in the dc discharge can impart large accelerations to the atoms. The integration in Eq. (64), where $\bar{y}_0$ is chosen so that $f(\bar{y}_0,\bar{v}_x,\bar{v}_y)$ is the initial distribution (45), is rather straigtforward; the remaining integrations in Eq. (63) can be carried out numerically and provide variations of Φ_{SS}^{expt} with the detuning and with the scaled width $w_S/2w_L$ for a given laser intensity. For each slit width w_S, the minimum of the dip Φ_{SS}^{expt} can be found and provides us with the required theoretical shift $\delta_L^{\min}$. Our predictions are compared with the experimental results in Fig. 6, showing quite a satisfactory agreement.

We discuss next the assumptions made. First, the conversion from slit aperture to interaction times relies on the fact that our atoms can be regarded as two-level systems. Because the light is linearly polarized everywhere, coherences between the ground Zeeman sublevels cannot build up and Eq. (65) still applies to our experimental situation provided we take as effective I_{sat} the two-level atom saturation intensity $\pi hc\Gamma/3\lambda_L^3$ and divide it by a suitable Clebsch-Gordan coefficient C that accounts for the multilevel structure of our ^{4}He atoms. For a π-excited $J=1\rightarrow J'=2$ transition the lower Zeeman sublevel steady-state populations are $p_0=3/5$, $p_{\pm 1}=1/5$, and C is the averaged square Clebsch-Gordan coefficient $2/3\times 3/5+1/2\times 2/5=0.6$. We note that for equally populated Zeeman sublevels the average squared Clebsch-Gordan coefficient turns out to be 0.56. Since the atoms enter the interaction region with equal populations in the three ground sublevels, the appropriate value should lie somewhere between 0.56 and 0.6.

VIII. CONCLUSIONS

We have studied the effects of light forces associated with atomic recoil on the fluorescence line shape in a common experimental setup for high-precision spectroscopy. Effects due to the recoil suffered by atoms during the interaction with a light beam are not new in laser spectroscopy, and among them the Lamb dip symmetric recoil splitting, a consequence of single-photon momentum transfer, is perhaps the most common one.

The line-shape modifications that we address here deal, however, with asymmetries and subsequent line-center shifts originating from cumulative cycles of absorption and emission processes. Our work complements that of previous publications concerned with line-center shifts observed in other spectroscopic configurations. These comprise the transverse excitation of a well collimated atomic beam by means of a traveling wave [20,7] and a standing wave [7], and the collinear excitation of a broad atomic beam by means of two traveling waves [21]. In the latter case, for instance, the line-center shift was observed by means of a frequency-modulated (weak) probe that propagated collinearly to the saturating (stronger) pump beam. In both types of traveling-wave excitation the atoms acquire a nonvanishing average velocity due to recoil, causing modifications of the initial atomic distribution function responsible for the line-shape asymmetry and concomitant line-center shift.

The experimental scheme that we examine in our work deals with the transverse excitation of the atomic beam, whereby a lin $\parallel$ lin standing-wave configuration is crossed at right angles by an effusive atomic beam. Atoms experience a transverse force whose nature and effect on their position and momentum distribution depend on the magnitude of the Doppler spread of the incident atomic beam. Such a spread may range from a few fractions of v_D (fluorescence spectroscopy regime) to several v_D (saturation spectroscopy regime) and atoms will experience correspondingly a *dipole* or a *radiation-pressure* force, i.e., a rectifying or a dissipative force [22]. Intermediate regimes are purposely not examined here as the corresponding fluorescence complex profile will have little relevance to the spectroscopic determination of atomic frequency separations. For small Doppler spreads we recover the well known redshift of the fluorescence peak first observed by Prentiss and Ezekiel [7]; in this case the atomic distribution function is modified by the transverse trapping due to the dipole force which tends to channel the atoms at the bottoms of the optical potential. For large Doppler spreads we predict a blueshift of the fluorescence Lamb dip; in this case the atomic distribution function is mostly modified by the Doppler transverse cooling (heating) [14] which tends to focus (defocus) the atoms in momentum space. These anticipations turn out to agree with the experimental observation of a Lamb dip line-center blueshift on ^{4}He, which we report in Sec. VII. The prediction for the magnitudes of the shifts, which can be as large as a few tenths of the natural transition linewidth, confirms our experimental results quite well.

Our calculations yield the analytical and closed-form results Eqs. (53) and (61) that provide a clear physical insight

into the origin of the line-center shifts and enable one to stress the basic differences between them. Both shifts decrease with the inverse of the atomic mass m, whereas blue- and redshifts grow, respectively, with the mean traversal time τ_0 and its square τ_0^2. Moreover, the shifts discussed here increase with increasing laser intensities, unlike those observed, e.g., in collinear excitation by two laser beams in low-pressure atomic ytterbium vapors [21]. The shifts increase owing to the increased height of the optical potential (fluorescence spectroscopy regime) and owing to the increased Doppler transverse cooling efficiency (fluorescence spectroscopy regime).

The expressions (53) and (61) are valid for short traversal times and suitably large atomic masses (see Table I) but do not suffer from any restriction on the laser light intensity. The result (61), in particular, complements and extends the detailed weak-field analysis of Grimm and Mlynek [4] on the collinear excitation of an atomic gas. The issue of the mean traversal time is a central one in the derivation of Eqs. (53) and (61) either when we reduce the atom-field evolution problem of the atomic distribution to the simplified kinetic equation (44), or when we carry out short-time perturbative expansions for the atomic distribution function. We take here times that are longer than the typical time scale Γ^{-1} for the internal degrees of freedom but shorter than a few ϵ_R^{-1}'s. The latter restriction enables us to use the perturbative expansions (49) and (57) and to avoid effects of momentum diffusion. Diffusion effects could be accounted for by including the term $D_{x,x}\partial^2 f/\partial^2 \overline{v_x}$ in Eq. (56). By further iterating such a modified Fokker-Planck equation, with the help of Eq. (57) and an appropriate expression for $D_{x,x}$ [13], one can see that the lowest-order diffusion contribution to the line shape (61) would be proportional to $\overline{\epsilon_R^3}\,\overline{\tau_0^2}$ and thus smaller, in the short-time limit, than the two other terms on the right hand side of Eq. (61). The model developed here strictly deals with a cycling atomic transition of a two-level atom. Consideration of multilevel atoms would induce modifications of the line-shape asymmetry and concomitant line-center shifts generally different from those discussed here. The inclusion of a Zeeman sublevel structure and open atomic transitions where optical pumping into nonradiative states would reduce the effective number of absorption-emission cycles performed by the atom clearly requires a more elaborate model, which will be the subject of future investigations.

Mechanical effects of light on atoms have been studied at length to the extent of manipulating the atom motion. This has led to the observation of interesting effects and many novel applications which encompass cooling and trapping as well as the fairly recent Bose-Einstein condensation of alkali-metal atomic vapors [23,24]. As well as the interest in light force owing to its potential applications, this topic provides an exciting area of fundamental research. It combines the internal quantum structure of atomic particles with their translational degrees of freedom in an essential way. The frequency shifts that emerge here in the attempt at improving the spectroscopic accuracy in the determination of fundamental constants and frequency standards are an unambiguous manifestation of this fascinating intertwining.

ACKNOWLEDGMENTS

We are grateful to R. Grimm and E. Arimondo for a critical reading of the manuscript and stimulating discussions over the various stages of the work. The work has been supported by the Instituto Nazionale per la Fisica della Materia (INFM).

APPENDIX A

The matrix recurrence relation (36) can be solved by a generalization of the continued fraction method. Under the assumption that H_n vanish for suitably large values of n, i.e., $\mathbf{H}_{n_c-1}=0$, the iteration of Eq. (36) from n_c-1 down to $n=1$ yields a continued fraction solution for the matrix $\mathbf{H}_0$ that can be written after some effort in the form

$$\mathbf{H}_0^{(2,3)}=\left(\frac{\Omega_0}{\Gamma}\right)^{-1}\cfrac{p_0}{1+\cfrac{p_1}{1+\cfrac{p_2}{1+\cfrac{p_3}{1+\cdots}}}},$$

$$\mathbf{H}_0^{(3,2)}=-\left(\frac{\Omega_0}{\Gamma S_R}\right)\cfrac{p_0'}{1+\cfrac{p_1'}{1+\cfrac{p_2'}{1+\cfrac{p_3'}{1+\cdots}}}}, \tag{A1}$$

$$\mathbf{H}_0^{(1,3)}=\left(\frac{\delta_L}{\Gamma}\right)\frac{2\mathbf{H}_0^{(2,3)}}{1+2iv_x v_D^{-1}},$$

with otherwise vanishing matrix elements. The numerators are given by

$$p_n=S_R\begin{cases}\dfrac{1+2inv_x v_D^{-1}}{1+i(n+1)v_x v_D^{-1}}\dfrac{\Gamma^2+4\delta_L^2}{\Gamma^2(1+2inv_x v_D^{-1})^2+4\delta_L^2} & (n=\text{odd})\\[2ex] \dfrac{1+2i(n+1)v_x v_D^{-1}}{1+inv_x v_D^{-1}}\dfrac{\Gamma^2+4\delta_L^2}{\Gamma^2[1+2i(n+1)v_x v_D^{-1}]^2+4\delta_L^2} & (n=\text{even}),\end{cases} \tag{A2}$$

while the p_n''s are obtained from Eq. (A2) by exchanging odd and even indexes. The highest-order term in the fraction expansion (A1) is clearly set by the cutoff value n_c; no substantial changes were observed by going beyond $n_c=6$, for the results discussed in this paper. This shows that H_n, as well as $X^{(n)}$, converges quite rapidly to zero, confirming the validity of the matrix continued fraction procedure [25].

APPENDIX B

The atomic distribution (64) can be derived by starting to divide the transverse section of the laser Gaussian beam into small and identical intervals $\bar{y}_n, \bar{y}_{n-1}, \bar{y}_{n-2}, \ldots$, where the atoms all move with the same constant velocity $\bar{v}_y$ and experience the same intensity. Within each small interval and for a sufficiently wide spread $\bar{\sigma}$, the lowest-order solution (62) applies and one obtains after repeated applications

$$
\begin{aligned}
f(\bar{y}_n,\bar{v}_x,\bar{v}_y) &\simeq f(\bar{y}_{n-1},\bar{v}_x,\bar{v}_y)\left(1-2\frac{\bar{\epsilon}_R}{\bar{v}_y}\int_{\bar{y}_{n-1}}^{\bar{y}_n}\partial_{\bar{v}_x}\bar{F}_x(\bar{y},\bar{v}_x)d\bar{y}\right)\\
&\simeq f(\bar{y}_{n-2},\bar{v}_x,\bar{v}_y)\left(1-2\frac{\bar{\epsilon}_R}{\bar{v}_y}\int_{\bar{y}_{n-2}}^{\bar{y}_{n-1}}\partial_{\bar{v}_x}\bar{F}_x(\bar{y},\bar{v}_x)d\bar{y}\right)\left(1-2\frac{\bar{\epsilon}_R}{\bar{v}_y}\int_{\bar{y}_{n-1}}^{\bar{y}_n}\partial_{\bar{v}_x}\bar{F}_x(\bar{y},\bar{v}_x)d\bar{y}\right)\\
&\simeq \cdots \simeq f(\bar{y}_0,\bar{v}_x,\bar{v}_y)\prod_{j=1}^{n}\left(1-2\frac{\bar{\epsilon}_R}{\bar{v}_y}\int_{\bar{y}_{j-1}}^{\bar{y}_j}\partial_{\bar{v}_x}\bar{F}_x(\bar{y},\bar{v}_x)d\bar{y}\right).
\end{aligned}
\tag{B1}
$$

Here we stop at some $\bar{y}_0$ where the form of the atomic distribution f is known. In the limit of infinitesimal small intervals we can replace the product in Eq. (B1) by an exponential to obtain

$$
f(\bar{y},\bar{v}_x,\bar{v}_y)=f(\bar{y}_0,\bar{v}_x,\bar{v}_y)\exp\left(-2\frac{\bar{\epsilon}_R}{\bar{v}_y}\partial_{\bar{v}_x}\int_{\bar{y}_0}^{\bar{y}}\bar{F}_x(\bar{y},\bar{v}_x)d\bar{y}\right). \tag{B2}
$$

[1] A. P. Kazantsev, G. I. Surdutovich, and V. P. Vakovlev, Pis'ma Zh. Éksp. Teor. Fiz. **43**, 222 (1986) [JETP Lett. **43**, 281 (1986)]; A. P. Kazantsev, G. A. Ryabenko, G. I. Surdutovich, and V. P. Yakovlev, Phys. Rep. **129**, 75 (1985).

[2] R. Grimm and J. Mlynek, J. Opt. Soc. Am. B **5**, 1655 (1988).

[3] R. Grimm and J. Mlynek, Phys. Rev. Lett. **61**, 2308 (1988).

[4] R. Grimm and J. Mlynek, Phys. Rev. A **42**, 2890 (1990).

[5] P. R. Hemmer *et al.*, Opt. Commun. **38**, 105 (1981).

[6] See, for instance, R. Gamidov, I. Taskin, and V. Sautenkov, in *Proceedings of the Fifth Symposium on Frequency Standards and Metrology*, edited by J. C. Bergquist (World Scientific, Singapore, 1996).

[7] M. G. Prentiss and S. Ezekiel, Phys. Rev. Lett. **56**, 46 (1986).

[8] For the Rydberg constant R_∞ see, e.g., B. de Beauvoir *et al.*, Phys. Rev. Lett. **78**, 440 (1997); T. Udem *et al.*, *ibid.* **79**, 2646 (1997).

[9] F. Minardi, G. Bianchini, P. Cancio Pastor, G. Giusfredi, F. S. Pavone, and M. Inguscio, Phys. Rev. Lett. **82**, 1112 (1999).

[10] For a review, see, e.g., D. J. E. Knight, in *Proceedings of EFTF97, Neuchatel, 1997* (FSRM, Neuchatel, 1997).

[11] C. Cohen-Tannoudji, in *Fundamental Systems in Quantum Optics*, Proceedings of the Les Houches Summer School of Theoretical Physics, Session LII, edited by J. Dalibard, J. M. Raimond, and J. Zinn-Justin (Elsevier, Amsterdam, 1991).

[12] J. Dalibard and C. Cohen-Tannoudji, J. Phys. B **18**, 1661 (1985).

[13] C. S. Adams and E. Riis, Prog. Quantum Electron. **21**, 1 (1997).

[14] C. Cohen-Tannoudji, J. Dupont-Roc, and Gilbert Grynberg, *Processus d'Interaction entre Photons et Atomes* (InterEditions/Editions du CNRS, Paris, 1988).

[15] A. Aspect, J. Dalibard, A. Heidmann, C. Salomon, and C. Cohen-Tannoudji, Phys. Rev. Lett. **57**, 1688 (1986).

[16] V. G. Minogin and O. T. Serimaa, Opt. Commun. **30**, 373 (1979).

[17] V. G. Minogin, Zh. Éksp. Teor. Fiz. **80**, 2231 (1981) [Sov. Phys. JETP **53**, 1164 (1981)]; V. S. Letokhov and V. G. Minogin, Phys. Rep. **73**, 1 (1981).

[18] R. Grimm and J. Mlynek, Appl. Phys. B: Photophys. Laser Chem. **49**, 179 (1989).

[19] P. Cancio Pastor, M. Artoni, G. Giusfredi, F. Minardi, F. S. Pavone, and M. Inguscio, in *Atomic Physics 16*, edited by W. E. Baylis and G. W. F. Drake, AIP Conf. Proc. No. 477 (AIP, Woodbury, NY, 1999).

[20] P. R. Hemmer *et al.*, Opt. Lett. **6**, 531 (1981).

[21] R. Grimm and J. Mlynek, Phys. Rev. Lett. **63**, 232 (1989).

[22] S. Stenholm, Eur. J. Phys. **9**, 242 (1988); Rev. Mod. Phys. **58**, 699 (1986).

[23] F. Dalfovo, S. Giorgini, L. Pitaeskii, and S. Stringari, Rev. Mod. Phys. **71**, 463 (1999).

[24] E. Cornell and C. Wieman, Sci. Am. (Int. Ed.) **278**, 26 (1998).

[25] H. Risken, *The Fokker-Planck Equation: Methods of Solution and Applications*, 2nd ed. (Springer, Berlin, 1989), pp. 78–129.